Effect of Nanoparticle Surface Coating on Cell Toxicity and Mitochondria Uptake

Hong Zheng[1], Luke J. Mortensen[2], Supriya Ravichandran[2], Karen Bentley[3], and Lisa A. DeLouise[1, 2, *]

[1] *Department of Dermatology, University of Rochester Medical Center, Rochester, New York 14642, USA*
[2] *Department of Biomedical Engineering, University of Rochester, Rochester, New York 14642, USA*
[3] *Department of Pathology and Laboratory Medicine, University of Rochester Medical Center, Rochester, New York 14642, USA*

We report on the effect of surface charge and the ligand coating composition of CdSe/ZnS core/shell quantum dot (QD) nanoparticles on human keratinocyte toxicity using fluorescent microscopy, flow cytometry, transmission electron microscopy. Two commonly reported positive charged (cysteamine, polyethylenimine) and two negative charged (glutathione, dihydrolipoic acid) ligands were studied. The QDs were fully characterized by UV-vis absorption spectroscopy, fluorescence emission spectroscopy, dynamic light scattering and zeta potential. Differences in surface coatings and charges were evaluated against cellular uptake, ROS generation, cytotoxicity, and mitochondrial targeting. Results show that the negative charged QDs coated with GSH exhibit excellent water solubility, high quantum yield and low cytotoxicity. Ligand composition is more important in ROS generation than surface charge whereas surface charge is an important driver of cytotoxicity. Most importantly we observe the selective accumulation of glutathione coated QDs in vesicles in the mitochondria matrix. This observation suggests a new strategy for developing mitochondria-targeted nanomaterials for drug/gene delivery.

KEYWORDS: *Quantum Dots, Keratinocytes, Endocytosis, Intracellular Localization, Mitochondria.*

Quantum dots (QDs) nanoparticles are powerful and versatile fluorescent probes for biomedical imaging and diagnostics, particularly for long-term, multiplexed, and quantitative detection.[1–4] The wide adoption of QDs as imaging tools in biology and medical research stems from the fact that they readily penetrate into cells without losing their unique photophysical properties, in particular, their size-tunable emission, high quantum yield, broad absorption spectrum, and resistance to photobleaching.[5–7] Owing to their small size, QDs nanoparticles can also penetrate physiological barriers, translocate, and accumulate in living organisms, and this has caused concern that exposure to certain types of nanoparticles may have significant adverse health effects.[8] Therefore, an understanding of the mechanism of cellular uptake and intracellular fate of QDs nanoparticles is a prerequisite for the safe use of nanotechnology to reap its potential benefits while limiting associated health hazards.

Recent investigations into the nature of the relationship between cellular uptake and physicochemical properties of QDs indicate that, in the absence of specific targeting, the entry of nanoparticles into cells and their cytosolic access are primarily governed by three factors: size, shape, and surface charge.[9–13] Given their size (5–6 nm), QDs cross the plasma membrane primarily through endocytosis, chiefly responsible for the uptake of cell nutrients and other small particles (<100 nm). Surface properties at the nanoscale strongly influence not only specific modes of internalization and subsequent subcellular localization, but also molecular and biological processes, including cell division and differentiation, ultimately dictating cellular fate.[14–16] It was shown that QD internalization can only occur if the concentration of QDs at the plasma membrane is sufficient.[17] The initial contact of QDs with cells, namely their interaction with the lipid bilayer and the surface proteoglycans, is controlled by the QD charge and concentration.[18] Since the proteoglycans are negatively charged, it is expected that positively charged QDs would be attracted toward the cell membrane by electrostatic interactions where they would readily accumulate facilitating internalization. Negatively charged QDs
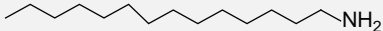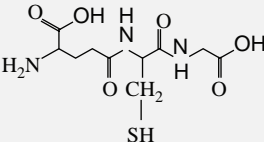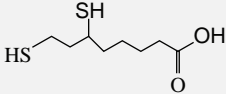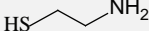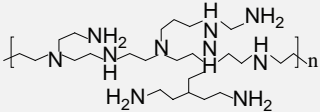
Table I. Structure and molecular weights (Mw) of the ligands used in this work.

Name	Structure	Mw (g/mol)
ODA		269.51
GSH		223.32
DHLA		208.34
CYS		77.15
PEI		25,000

would be weakly bound to the lipid bilayer and thus less readily taken up. However, the impact of surface charge on cellular uptake of non-targeted QDs has been studied sporadically and the results have so far been inconsistent. Some papers in fact report that negatively charged QDs get into cells more efficiently than positively charged QD[19–23] while others report that positively charged QDs are endocytosed.[24] Still other studies showed surface coating/charge has no effect on QD endocytosis.[25] Hence, nanoparticle endocytosis maybe cell type specific and/or very sensitive to nanoparticle properties including ligand composition for which very few systematic studies exist.

In this study we used the same nanoparticle core to systematically quantify the impact of surface ligand composition and charge on the optical properties of fluorescent QDs and their cellular interaction with a goal to discover a coating that provides superior colloidal stability, high optical quality and low cytotoxicity. We examined cell uptake and toxicity of QDs having a CdSe/ZnS core/shell coated with two commonly used positive ligands, cysteamine (CYS) and polyethylenimine (PEI) and two negative ligands, glutathione (GSH) and dihydrolipoic acid (DLHA). The structure and molecular weights of the four surface coatings are listed in Table I. Experiments were performed using human keratinocytes (HaCaT cell line). QD internalization was observed by transmission electron microscopy (TEM) and a MitoTracker dual staining protocol. The extent of QD cell association was estimated by fluorescence microscopy and flow cytometry. The results showed that negatively charged QDs enter cells less efficiently with lower reactive oxygen species (ROS) generation and cytotoxicity than positively charged QDs. We also show that targeting and accumulation of GSH-modified QDs nanoparticles in mitochondria occurs in HaCaT cells.

The findings reported here provide important insight into the mechanisms nanoparticle cytotoxicity and guidance for the design of mitochondria-targeted nanomaterials for drug/gene delivery systems.

MATERIALS AND METHODS
Materials
Commercial CdSe/ZnS octadecylamine (ODA)-capped QDs suspended in hexane with emission at 620 nm and core/shell diameter of 6.2 nm (NN-Labs, Fayetteville, AR) were used in this study. Glutathione (GSH, 98%), thioctic acid (98%), cysteamine hydrochloride (CYS, 98%), polyethylenimine (PEI, MW 25,000) and tetramethylammonium hydroxide (99%) were purchased from Sigma-Aldrich. Other organic solvents used were of analytical reagent grades.

LIGAND EXCHANGE OF QD COATING
Preparation of Dihydrolipoic Acid
Dihydrolipoic acid (DHLA) was freshly prepared through the deoxidation of thioctic acid by $NaBH_4$ according to the literature method.[24, 26, 27] Briefly, to a 19.5 ml of 0.25 M $NaHCO_3$ solution containing 1.0 g of thioctic acid, a total of 0.2 g of $NaBH_4$ was added. The mixture was vigorously stirred and kept in a cold bath (0–5 °C). After 2 h, 16.7 ml of toluene was added and a two-phase solution resulted. The colorless solution was acidified to pH 1 with HCl solution. The reduced thiotic acid was fully into the organic phase resulting in a whitish milky appearance. The organic phase containing the product (reduced thiotic acid) was isolated, collected and then dried over anhydrous magnesium sulfate. The organic solvent was removed and 0.9 g DHLA was produced with a yield of 89%.

Preparation of GSH and DHLA Capped CdSe/ZnS QDs
Carboxylated-CdSe/ZnS QDs were synthesized by cap exchange with thiol ligands including GSH and DHLA to provide a stable negative QD surface. Briefly, the thiol ligand (20 mg of GSH or DHLA) was added to methanol (1 mL) and the pH of the solution was adjusted to 11 with tetramethylammonium hydroxide pentahydrate $((CH_3)_4NOH \cdot 5H_2O)$. The ODA-QDs in hexane were precipitated by addition of methanol:acetone (1:1) and separated by centrifugation at 14,000 rpm for 5 min at room temperature. Then the ODA-QDs were redispersed in tetrahydrofuran (THF). The thiol ligand methanol solution (20 mg/mL, 1 mL) was slowly added to the ODA-QD THF solution (0.25 μM, 200 μL) at room temperature in a small glass vial. The mixture was stirred at 60 °C for 2 h and precipitated with the addition of ether by centrifugation at 14,000 rpm for 5 min at room temperature. The supernatant was discarded and the QD sample was redispersed in 200 μL deionized water. The QDs were dialyzed

using a 5 kD molecular weight cutoff DispoDialyzer filter (Harvard Apparatus Inc.) and 500× excess volume of water for 72 hours with water changing every 24 hours. After dialyzing, the QD concentration was determined by measuring the absorption at the first excitation and using an extinction coefficient from the literature with Lambert-Beer's law.[26]

Preparation of CYS-Capped CdSe/ZnS QDs

Amino-CdSe/ZnS QDs (CYS-QDs) were synthesized according to a previously reported method.[30] Briefly, cysteamine hydrochloride (50 mg) was added to a small glass vial and heated at 80 °C. After melting, a solution of ODA-QDs diluted in THF (0.25 μM, 500 μL), prepared as described above, and slowly added to the vial and heated at 80 °C for 2 h. After, the sample was flushed with a N_2 stream to remove any residual organic solvent and then the CYS-QDs were redispersed in 200 μL deionized water. The QDs were dialyzed using a 5 kD molecular weight cutoff DispoDialyzer filter (Harvard Apparatus Inc.) and 500× excess volume of water for 72 hours with water changing every 24 hours. After dialyzing, the concentration is determined by measuring the absorption at the first excitation and using an extinction coefficient from the literature with Lambert-Beer's law.[26]

Preparation of PEI-Capped CdSe/ZnS QDs

Amino-capped CdSe/ZnS QDs (PEI-QDs) were synthesized through direction ligand-exchange reaction.[24] Briefly, the PEI (MW = 25 kD, branched) was first dissolved in THF at a concentration of 80 mg/mL. PEI THF solution (0.5 mL) was slowly added to the THF ODA-QD solution (0.25 μM, 400 μL) prepared as described above. The mixture was stirred overnight at room temperature and the product formed appeared as sticky semisolid. The sample was flushed with N_2 stream to remove any residual organic solvent and then the PEI-QDs were redispersed in 400 μL deionized water. Finally, the resulting aqueous suspension of QDs was centrifuged (14,000 rpm for 5 min) and washed twice with deionized water. After washing, the concentration was determined by measuring the absorption at the first excitation and using an extinction coefficient from the literature with Lambert-Beer's law.[26]

CHARACTERIZATION OF QDs
Optical Characterization

UV/Vis absorption spectra were measured at room temperature with a Shimadzu UV-1601PC spectrophotometer (Shimadzu Scientific Instruments, Inc. Columbia, MD, USA) and photoluminescence (PL) spectra were collected with a modular Acton Research fluorometer equipped with a Ge detector, respectively. PL spectra were taken at the excitation wavelength $\lambda_{ex} = 488$ nm and at the excitonic absorption peak for PL quantum yields. Rhodamine 6G was used as a standard for determining PL quantum yield (QYs).

Hydrodynamic Size Measurements

Hydrodynamic size of QD was evaluated by using Dynamic Light Scattering (DLS). DLS measurements were performed using a Malvern Nano-ZS zetasizer (Malvern Instruments Ltd., Worcestershire, United Kingdom). The Nano-ZS employs non-invasive back scatter (NIBS™) optical technology and measures real time changes in intensity of scattered light as a result of particles undergoing Brownian motion. The sample is illuminated by a 633 nm Helium-Neon laser and the scattered light is measured at an angle of 173° using an avalanche photodiode. The size distribution is calculated from the diffusion coefficient of the particles according to Stokes-Einstein equation. The average diameter and the polydispersity index of the samples are calculated by the software using CONTIN analysis.

Zeta Potential Measurements

The zeta potential of QD was measured with the Malvern Nano ZS using the technique of Laser Doppler Velocimetry (LDV). In this technique, a voltage is applied across a pair of electrodes at either end of the cell containing the particle dispersion. Charged particles are attracted to the oppositely charged electrode and their velocity was measured and expressed in unit field strength as an electrophoretic mobility. The zeta potential was calculated from the electrophoretic mobility using Henry's equation and built in software.

TREATMENT OF CELLS WITH QDs
Cell Line

The human keratinocytes cell line HaCaT were cultured in high-glucose Dulbecco's modified Eagle's medium (DMEM). Media contained 10% fetal calf serum, streptomycin (1 mg/mL) and penicillin (1000 units/mL). All cells were cultured at 37 °C in water-saturated air supplemented with 5% CO_2. Culture media were changed every three days. Cells were passaged once a week. Cells in the exponential growth phase were used for experiment.

Flow Cytometric Determination of Oxidative Stress and QDs Uptake

HaCaT cells were plated in 12-well plates and then incubated up to about 48 h and grow to about 80% confluence before experiments. The medium was replaced by DMEM (1.5 mL) containing 10 nM of GSH-, DHLA-, CYS- or PEI-capped QDs, and cells were incubated for 24 h at 37 °C, followed by staining with 10 μM 2′,7′-dichlorodihydrofluorescein diacetate (DCF-DA, Invitrogen, Grand Island, NY) for 30 min at 37 °C. The cells were then trypsinized with 0.25% trypsin-EDTA. The samples were then centrifuged and the pellet fixed in 3% Formalin. Appropriate controls and single-stain controls for compensation were included in each experiment. At least 20,000 cells were analyzed per group using BD LSR II flow

cytometry (Becton–Dickinson) at an excitation wavelength of 488 nm and emission wavelengths of 515 for DCF-DA, at an excitation wavelength of 405 nm and emission wavelengths of 605 for fluorescence profile of the QD-associated cells, respectively. Results from flow cytometry were analyzed using the Flow Jo (Version 7.5) software.

Determination of QD Uptake by Spectrofluorometry

HaCaT cells were plated in 12-well plates and then incubated up to 48 h and grown to about 50% confluence before experiments. The medium was replaced by DMEM (1.5 mL) containing 10 nM of GSH-, DHLA-, CYS-, or PEI-capped QDs, and cells were incubated for 24 h at 37 °C. At the end of the incubation, the medium was removed. The cells were fixed in 3% Formalin and analyzed under a fluorescence microscope (Olympus IX70 with QImaging Retiga EXi camera) at 40× magnification with images obtained under bright field and fluorescent filters (DCF-DA, excitation 480 nm/emission 510 nm; QD, excitation 360 nm/emission 620 nm). Images were analyzed using ImageJ.

Cell Viability (MTT Assay) of QDs

HaCaT cells were plated in 12-well plates and incubated with 10 nM GSH-, DHLA-, CYS-, or PEI-capped QDs for 24 hr as described above. After incubation the cell culture media was removed and the MTT agent in media was added. The MTT agent was dissolved in PBS (5 mg/ml) and added to the cell media in a 1:10 dilution medium and the plates were incubated for ~4 hr. Thereafter, the media was replaced with 0.4 ml of acidic isopropyl alcohol (0.04 M HCl in absolute isopropyl alcohol) to solubilize the Formazan crystals. The absorbance of the resulting solutions was read at 600 nm wavelength in microplate reader.

TEM Studies on the Cellular Uptake of QDs

HaCaT cells were co-cultured with the 10 nM of GSH-, DHLA-, CYS-, PEI-capped QDs for 24 h as described above. To investigate the location of the QDs in the HaCaT cells, the cells were prepared for TEM analysis. The cells were fixed with 2.5% glutaraldehyde in 0.1 M, pH 7.2 cacodylate buffer for 24 h at 4 °C and rinsed with cold 0.1 M pH 7.2 cacodylate buffer three times. The cells were then fixed with 1% osmium tetraoxide (Ted Pella, Inc.) for 1 h at 4 °C and washed with cold distilled water three times. The cells were dehydrated using graded alcohol baths (25%, 50%, 75%, and 100%) and then infiltrated with and embedded in Spurr epoxy resin with overnight polymerization at 70 °C. After embedding, the samples were cut to 1–2 μm with a glass blade and finally sliced at 70 nm with a diamond knife and placed on copper grids. Nanoparticle localization was evaluated using a Hitachi 5100 TEM apparatus.

Intracellular Localization of QDs on Cells Using the Dual Staining Protocol

HaCaT cells were co-cultured with 10 nM of GSH-, DHLA-, or PEI-capped QDs for 24 h. The culture medium was then removed and replaced with medium pre-warmed to 37 °C containing MitoTracker Green (Invitrogen, OR, USA) to a final concentration 100 nM. Cells were incubated with the dye for 30 min, then replaced with fresh medium. Finally, the cells were observed under fluorescence microscope (Olympus IX70 with QImaging Retiga EXi camera) fitted with the correct filter set. Images were recorded separately in each fluorescence channel and merged afterwards. Images were analyzed using ImageJ.

RESULTS AND DISCUSSION

Measurement of UV/Vis Absorption Spectra and Photoluminescence Spectra

We examined the optical characteristics of the QD nanoparticles by measuring their absorption and fluorescence spectra. Figure 1 shows a comparison of the
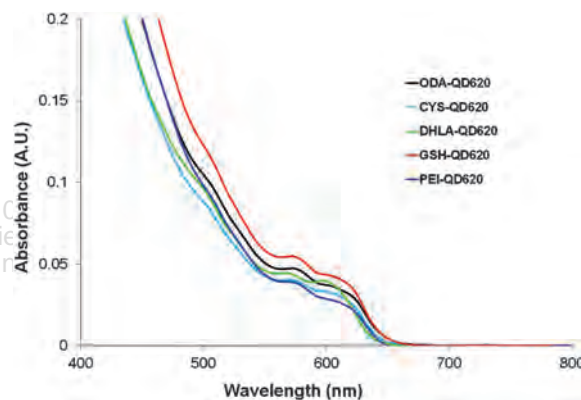

Figure 1. Comparison of the UV/Vis absorption spectra for the solvent soluble ODA capped QDs and the four different water soluble ligand capped QDs. All solutions were 8 μM. Results show very little change in the absorption properties.
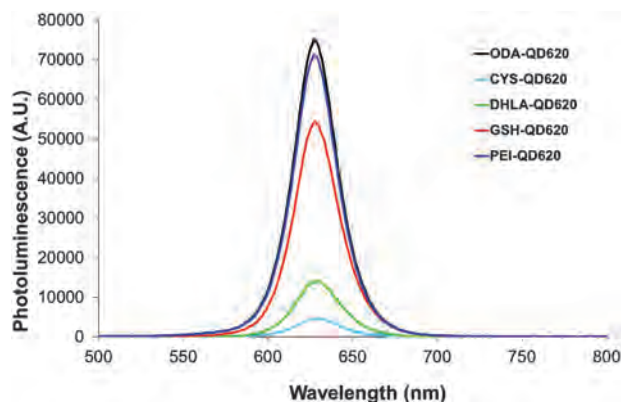

Figure 2. Comparison of the photoluminescence (PL) spectra for the solvent soluble ODA capped QDs and the four different water soluble ligand capped QDs. All solutions were 8 μM. Results show very little change in the PL peak wavelength or shape but differences exist in quantum yield.

Table II. Dynamic light scattering and quantum yield results.

Sample	Quantum yield (%)	Zeta potential (mV)[a]	Hydrodynamic diameter (nm)[a]	PDI[b]
ODA-QDs	56.0	N/A	N/A	N/A
GSH-QDs	40.7	-23.8 ± 0.71	20.9 ± 1.51	0.44 ± 0.04
DHLA-QDs	10.6	-26.2 ± 7.18	13.6 ± 0.71	0.49 ± 0.18
PEI-QDs	53.4	29.8 ± 0.35	26.7 ± 5.69	0.44 ± 0.14
CYS-QDs	6.5	35.3 ± 0.25	15.7 ± 0.95	0.40 ± 0.11

Notes: [a]Measured with 0.1 mg mL^{-1} of QDs in DI water (pH = 6.6). Results are expressed as means $\pm$ SD ($n = 3$); [b]Polydispersity expressed as means $\pm$ SD ($n \leq 5$).

absorption spectra for the different water soluble ligand capped QDs (PEI-, CYS-, DHLA-, GSH-) at equivalent molar concentration (8 μM) compared to the solvent soluble ODA capped QD starting material. Changes in UV/Vis absorption spectra for the different ligand capped QDs are comparatively small. This suggests a high stability of the QD core/shell and that the ligands and ligand exchange protocols had no adverse effect on the QD
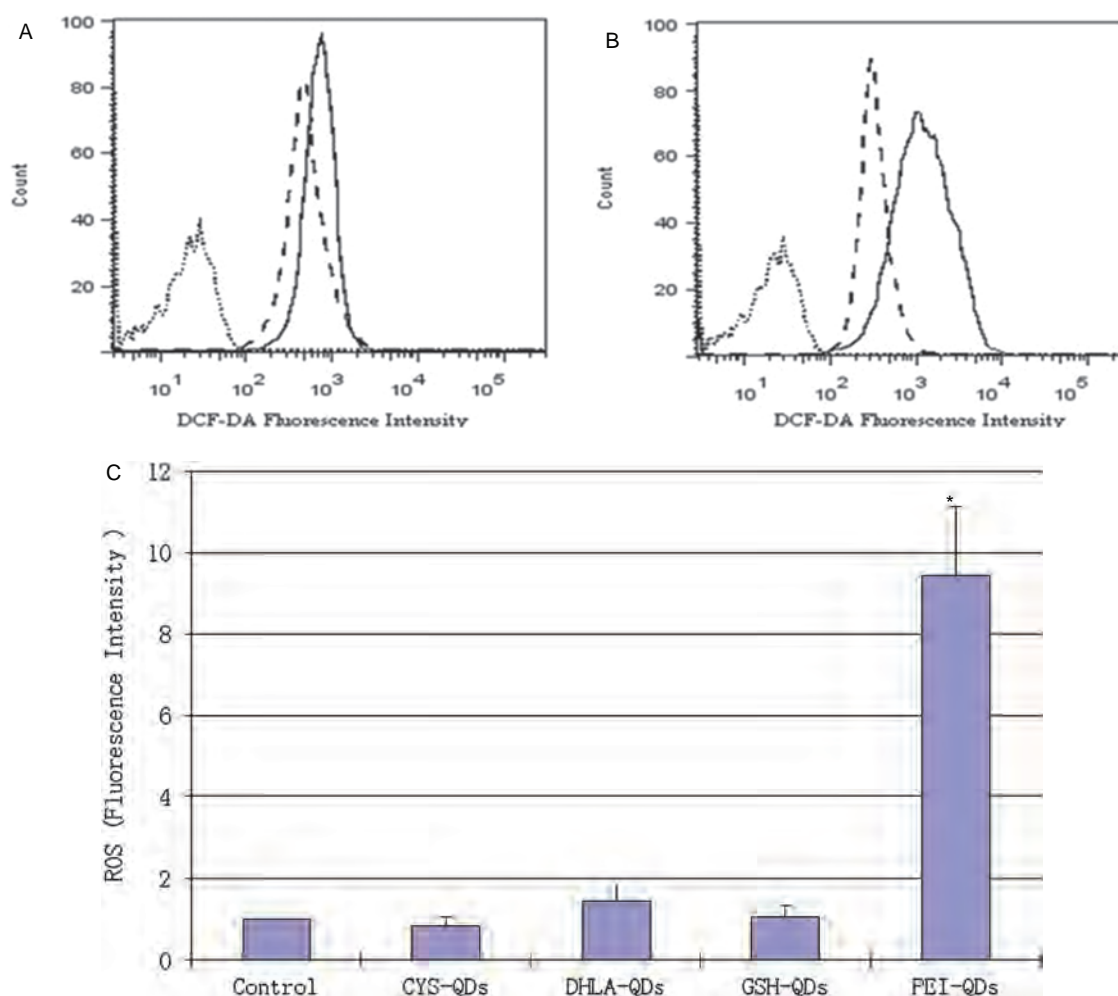

Figure 3. ROS generation in HaCaT cells exposed to negative and positive charged QD assessed by flow cytometry. Representative examples of flow cytometry data showing ROS levels in (A) in HaCaT cells exposed to GSH-QDs (dash line) and DHLA-QDs (solid line); dotted line shows untreated cells and (B) HaCaT cells exposed to CYS-QDs (dash line) and PEI-QDs (solid line); dotted line shows untreated cells. (C) Summary comparison of ROS generation for different ligands capped QDs (GSH-, DHLA-, CYS-, PEI-QDs) in HaCaT cells. ROS levels were determined by the DCF-DA as described in Section 2. Cell cultures were treated with different ligands capped QDs and ROS production was measured as fluorescence intensity. Results are expressed as means $\pm$ SD ($n = 3$). * indicates significant differences between treated and untreated cell culture ($p < 0.05$).

molar extinction and UV/Vis absorbance. Figure 2 shows the photoluminescence (PL) spectrum for the different water soluble ligand capped QDs at equivalent molar concentration (8 μM) compared to the solvent soluble ODA capped QD starting material. Results show that the photoluminescence (PL) spectra shape and peak wavelength change very little as function of the ligands again suggesting a high stability of the QD core/shell and that the ligands and the ligand exchange protocols had no adverse effect on the QD core/shell size or stability. However, the magnitude of the QD quantum yield (PL peak height) is highly impacted by the ligand composition as discussed below.

Size, Surface-Charge and Quantum Yield

Dynamic light scattering (DLS) was used to measure the size, polydispersity index (PDI) and zeta potential of the water soluble ligand capped QDs (PEI-, CYS-, DHLA-, GSH-). Quantum yields were measured relative to Rhodamine 6G with excitation at 488 nm. Results listed in Table II show that the positive charge PEI-QDs and the negative charge GSH-QDs are slightly larger in
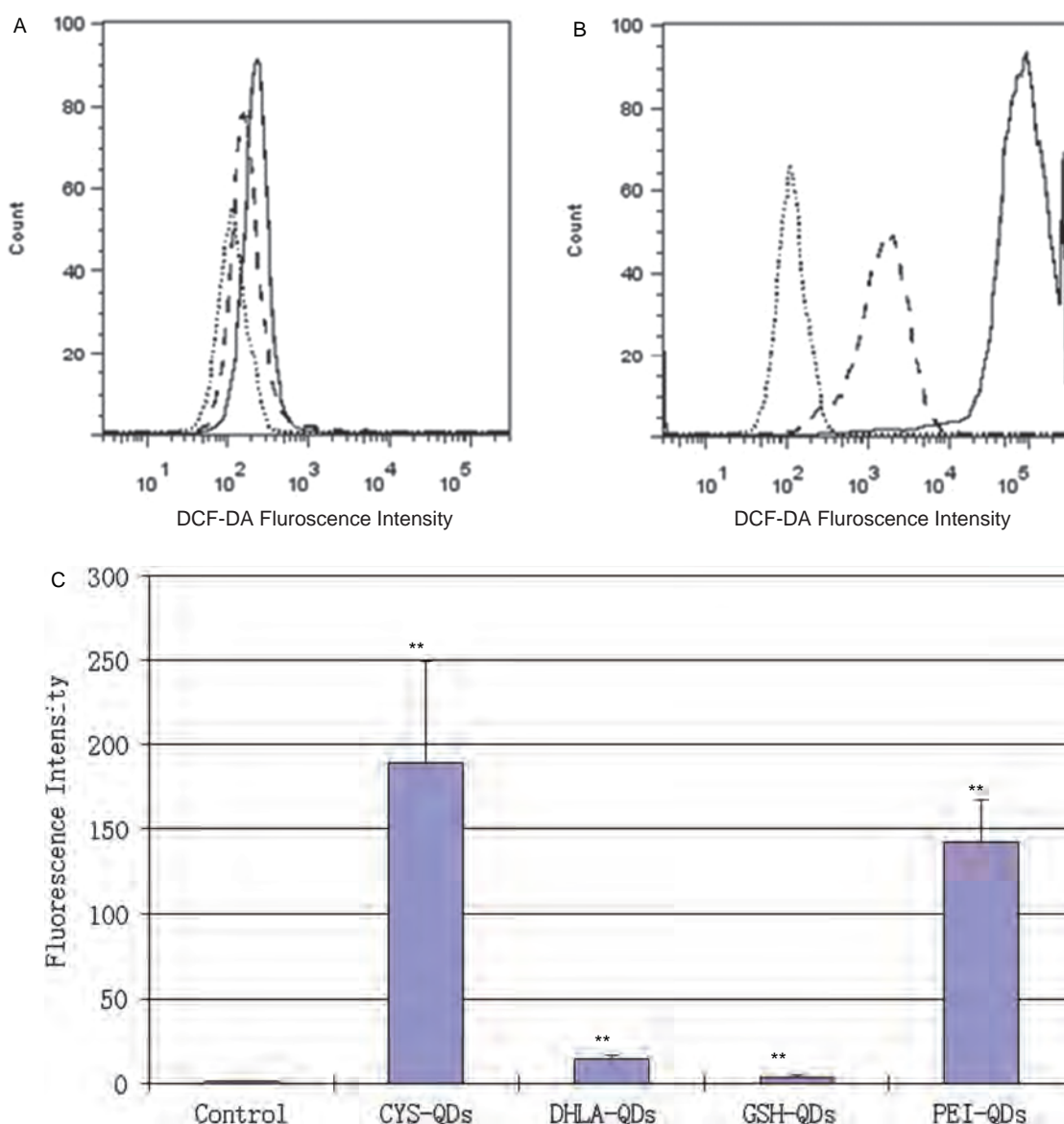

Figure 4. Negative and positive charged QD association with HaCaT cells assessed by flow cytometry. Representative examples of flow cytometry data showing QD association (A) with HaCaT cells exposed to GSH-QDs (dash line) and DHLA-QDs (solid line); dotted line shows untreated cells and (B) with HaCaT cells exposed to CYS-QDs (dash line) and PEI-QDs (solid line); dotted line shows untreated cells. (C) Summary comparison of QD cellular association for the different water soluble ligands capped QDs (GSH-, DHLA-, CYS-, PEI-QDs), (*n* = 3). Data are expressed as fluorescence intensity units. ** indicate significant differences between treated and untreated control cell culture (*p* < 0.001).

hydrodynamic size and have the highest photoluminescence quantum yield (QY).

Dependence of ROS Generation in HaCaT Cells on the Water Soluble Ligand QD

We detected the generation of ROS in HaCaT cells following a 24 h exposure to each of the four water soluble ligand capped QDs using the DCF-DA flow cytometry assay. Figure 3(A) shows a comparison of representative flow cytometry ROS intensity plots for the two negative charged ligands, DHLA-QD and GSH-QDs, relative to untreated cells. Results show that the GSH-QDs produced less ROS than DHLA-QDs. Figure 3(B) shows a comparison of representative flow cytometry ROS intensity plots for the two positive charge ligands, CYS-QD and PEI-QDs, relative to untreated cells. Results show that positive charge PEI-QDs produced more ROS than the positive CYS-QDs. Although the CYS-QDs are more positively charged, CYS is a thiol-based antioxidant ligand that may help suppress the average ROS. Figure 3(C) shows a summary comparison ($n = 3$) of the ROS intensity clearly indicating that the positive charged PEI-QDs induce the highest cellular stress. This suggests that ligand composition is more important in generating ROS cellular stress than surface charge as the CYS-QDs are more positively charged (Table II) then the PEI-QDs but they produce much less ROS.

Determination of QD Cellular Association Using Flow Cytometry

A quantitative measure of QD cellular association was determined using flow cytometry. Figure 4(A) shows a comparison of representative flow cytometry fluorescence intensity plots for the two negative charged QDs. Results indicate that the cells have slightly higher DHLA-QD association compared to GSH-QD. Figure 4(B) shows a representative comparison of the flow cytometry fluorescence intensity plots for the two positively charged QDs. Results indicate that the PEI-QDs associate with cells to a much greater extent that the CYS-QDs. Figure 4(C) shows a summary comparison of the HaCaT cell associated fluorescence intensity for the water soluble QDs. Results show that on average ($n = 3$) the positive charge ligands capped QDs (PEI-QDs, CYS-QDs) associate with cells more than negative charge QDs (GSH-QDs, DHLA-QDs).

Determination of QD Cellular Association Using Fluorescent Microscopy

The association of the four water soluble ligand coated QDs (GSH-, DHLA-, CYS-, PEI-QDs) with HaCaT cells after 24 h incubation was assessed by fluorescence microscopy (Fig. 5). This qualitative measure of cell association is consistent with the flow data that clearly shows that after extensive washing the positively charged QDs (PEI-QDs, CYS-QDs) retain a significantly higher cell association than the negatively charged QDs (GSH-QDs, DHLA-QDs). No obvious changes in cell
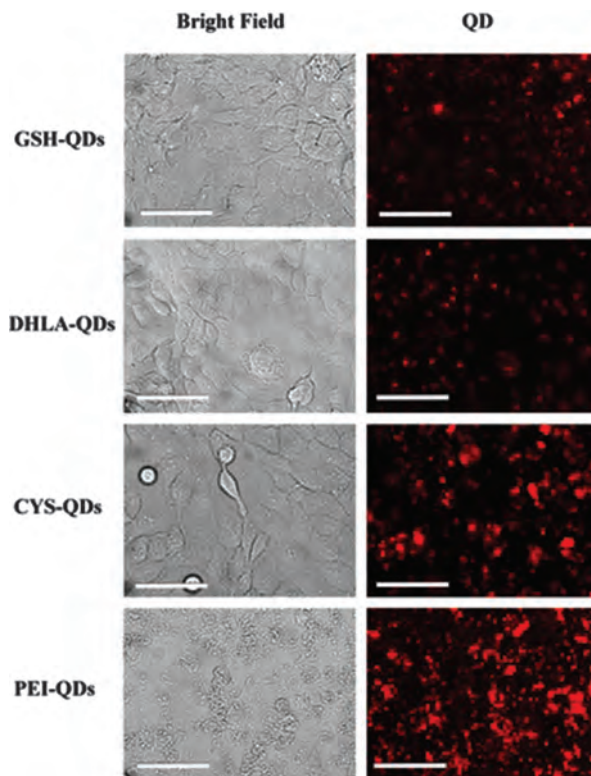

Figure 5. Assessment of QDs coated with different ligands induce uptake by HaCaT cell using fluorescence microscope after 24 h incubation with HaCaT cells (Scale bar: 25 μm).

morphology are evident following 24 h QD incubation with the exception of the PEI-QDs which appears to induce some cell granularity which maybe a sign of cytotoxicity.

Assessment QD Exposure on HaCaT Cell Viability

Cationic nanoparticles are often associated with significant cytotoxic effects, due to their electrostatic interactions with
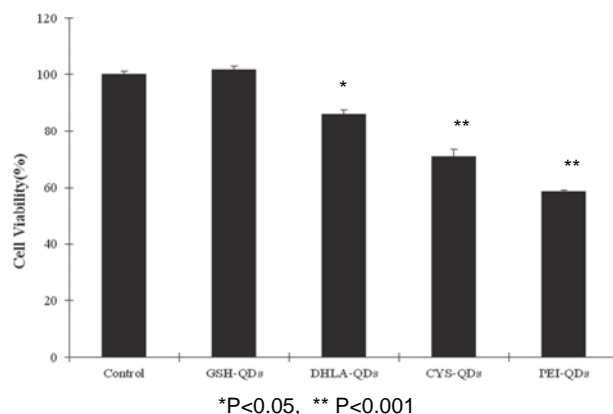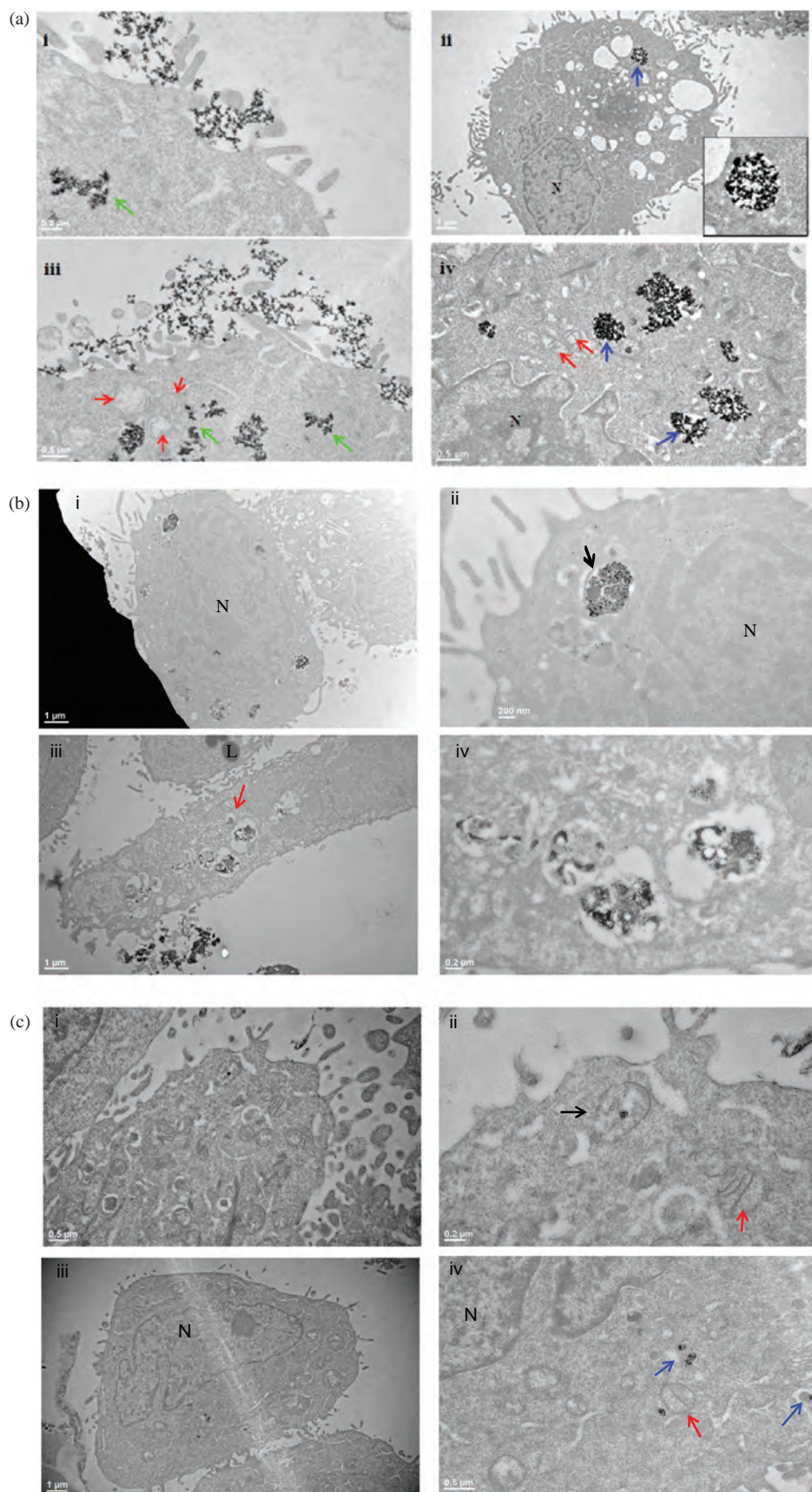

Figure 6. HaCaT cell viability data for (10 nM) QDs coated with different positive and negative charge ligands for 24 h using standard MTT colorimetric assay ($n = 3$).
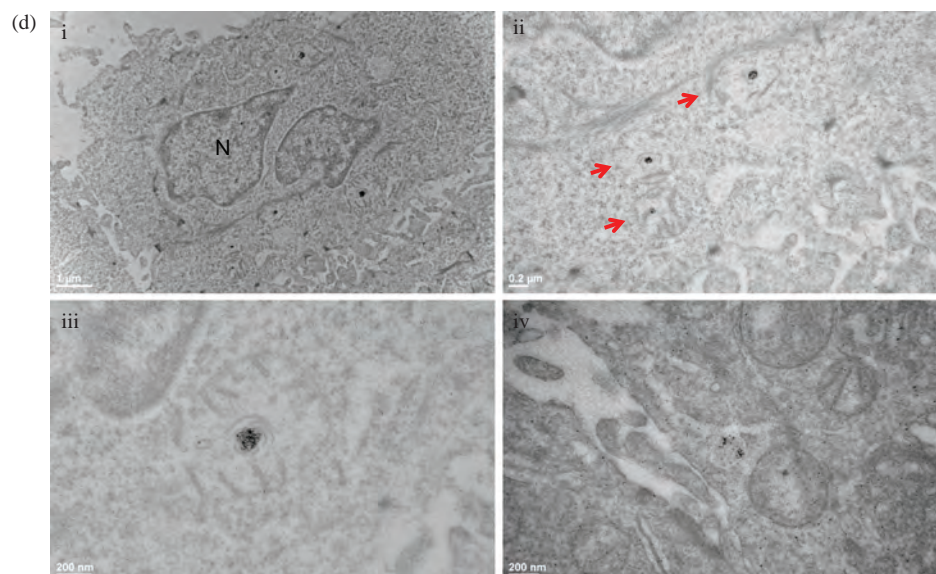
Figure 7. Continued.

Figure 7. **(a)** TEM images illustrating the cellular uptake and intracellular translocation of positively charged CYS-QDs. **(i)** Endocytosis of CYS-QD aggregates into a vesicle at plasma membrane is evident. **(ii)** Maintenance of CYS-QD aggregates in spherical vesical is evident (blue arrows). Inset shows magnified view of the vesical containing CYS-QDs. **(iii)** Once internalized the CYS-QD aggregates appear to disrupt the vesicle that contained them and they appear to localize in the cytosol as free aggregates (green arrows). **(iv)** There was no evidence for accumulation of CYS-QDs in the nucleus (N) or uptake into mitochondria (red arrows). **(b)** TEM images illustrating the cellular uptake and intracellular translocation of positively charged PEI-QDs. **(i)** HaCaT cells appear to sequester PEI-QD aggregates in cytosolic vesicles. **(ii)** Enlarged view of vesicle showing distinct membrane (arrow). **(iii)** Unlike vesicles containing CYS-QDs, quite often the vesicles containing PEI-QDs appear fluid filled. HaCaT cells also appear to produce much more lipid droplets (L); grey circles. **(iv)** Enlarged view of fluid filled vesicles containing PEI-QDs. There was no evidence for penetration or accumulation of PEI-QDs in nucleus (N) or uptake into mitochondria (red arrows). **(c)** TEM images illustrating the cellular uptake and intracellular location of negatively charged DLHA-QDs. **(i)** In comparison to positive charged QDs (CYC, PEI), much fewer instances of negative charged DHLA-QD aggregates were present in HaCaT cells. **(ii)** Enlarged view of image in (i) showing small clusters of DLHA-QDs in a vesicle with a distinct membrane (black arrows). **(iii)** Another example of a HaCaT cell with small DHLA-QD clusters. **(iv)** Enlarged view of image in (iii) showing small DHLA-QD clusters (blue arrows). There was no evidence for accumulation of PEI-QDs in nucleus (N) or uptake into mitochondria (red arrows). **(d)** TEM images illustrating the cellular uptake and intracellular location of negatively charged GSH-QDs. **(i)** Similar to the negative charged DHLA-QDs there are much fewer instances of cytosolic clusters of GSH-QDs compared to the positive charged QDs (CYS, PEI) in HaCaT cells. Interestingly, we find that the preponderance of GSH-QD cytosolic clusters localize in the mitochondria. **(ii)** Enlarged view of image (i) showing small GSH-QDs clusters in mitochondria (red arrows). **(iii)** Enlarged view of image (i) showing small GSH-QDs clusters in mitochondria. GSH-QDs appear sequestered in a vesicle in the mitochondria matrix. **(iv)** Some GSH-QD clusters also localize into vesicles. There was no evidence for accumulation of GSH-QDs in the cell nucleus (N).

negatively charged glycocalyx on cell membranes.[27] It is thus important to evaluate the toxicity profiles for QDs with different charge and coating using standard cytotoxicity assays. Figure 6 shows cell viability data obtained from exposure to the four types of QDs at the same 10 nM molar concentration, together with a control (no QDs) for comparison. The results show that the PEI-QDs are the most cytotoxic whereas the GSH-coated dots exhibit negligible toxicity under the same exposure conditions. The fact that the negatively charged DHLA-QDs exhibit some toxicity indicates that coating composition as well as charge impacts cytotoxicity. One possible reason for the negligible GSH-QD toxicity effect is that the GSH tripeptide (γ-L-glutamyl-L-cysteinylglycine) is an endogenous antioxidant thiol compound that exists in most cells and is known detoxify Cd^{2+} ions at the cellular level due to its chelating capability.[28] In contrast, the positively charged QDs are likely to move across cell membranes through

rapid endocytosis; PEI is widely exploited as a gene delivery vector.[29]

Imaging of the Intracellular Localization of QDs on Cells by TEM

To shed light on the effect of surface charge and coating composition on the internalization of QDs by cells and their intracellular translocation, HaCaT cells were incubated with 10 nM of the four different ligand coated QDs (GSH-, DHLA-, CYS-, PEI-QDs) for 24 h and the cells were prepared for TEM imaging (Fig. 7). From the above work we found that positive charged (PEI, CYS) QDs exhibit higher cell association than the negative charge (GSH, DHLA) QDs and that the PEI-QDs generate higher ROS and cytotoxicity levels than the more positively charged CYS-QDs. The TEM results are consistent with these observations. Representative TEM images of HaCaT cells exposed to CYS-QDs (Fig. 7(a)) show

distinct presence of dark punctate spots and large aggregates of CYS-QDs. These features are not presence in control cells not exposed to QD. Endocytosis of CYS-QD aggregates into vesicles occur at the plasma membrane. Maintenance of CYS-QD aggregates in spherical vesicles is evident but there are also many instances where CYS-QD aggregates appear to be localized in the cytosol as free aggregates suggesting that once internalized the strong positive charge disrupts the vesicle membrane. There was no evidence for accumulation of CYS-QDs in the nucleus (N) or uptake into mitochondria. HaCaT cells exposed to PEI-QDs (Fig. 7(b)) generally appeared less healthy and finding intact cells to image proved challenging. Analysis of intact HaCaT cells found PEI-QD aggregates sequestered in cytosolic vesicles with distinct membranes. However, unlike CYS-QDs, the vesicles containing PEI-QDs appeared fluid filled. This is likely due to the excessive positive charge and the proton sponge effect that changes the osmolarity of vesicles resulting in endosomal swelling and rupture.[30] HaCaT cells also appear to produce many more lipid droplets which is a characteristic of apoptosis and cellular stress.[31] There was no evidence for nuclear penetration or accumulation of PEI-QDs or uptake into mitochondria. TEM analysis of HaCaT cells exposed to the negative charged DHLA-QD (Fig. 7(c)) and GSH-QDs (Fig. 7(d)) show considerably less QD cell uptake than the positive charged QDs (PEI, CYS) which is consistent with the less ROS and cytotoxicity observed.

The DHLA-QDs were present in vesicles as small cytosolic clusters with no strong evidence for nuclear or mitochondria association. Whereas, we interestingly observed that the preponderance of GSH-QD clusters were localized in the mitochondria.

GSH is a key cytosolic peptide that serves as a cofactor for a number of antioxidant and detoxifying enzymes. While synthesized exclusively in the cytosol, specific carriers exist to import GSH to the mitochondria to defend against oxidative stress.[32, 33] It is plausible that these carriers facilitated sequestration of GSH-QDs into mitochondria but without disrupting the respiratory chain or causing overt cytotoxicity. This is in contrast to reports on other nanoparticle types such as starch-coated silver nanoparticles which were found inside mitochondria and suggested to be a cause of the observed cytotoxicity and genotoxicity.[34] It is interesting to note from Figure 7(d)(iii) that it appears the GSH-QD cluster is sequestered in a double membrane vesicle in the mitochondria matrix. Vesicular budding from mitochondria and transport to cytosolic peroxisomes and lysosomes is known to be a mechanism that mitochondria use to remove oxidized protein and lipid by-products from respiration[35] but to our knowledge mitochondria do not contain the machinery required for vesicular endocytosis (e.g., *t*-snares). However, mitochondria and plasma membrane caveolae are closely apposed in many cell types and these caveolae have been suggested as a means to traffic cargo into mitochondria.[36] It is unclear at
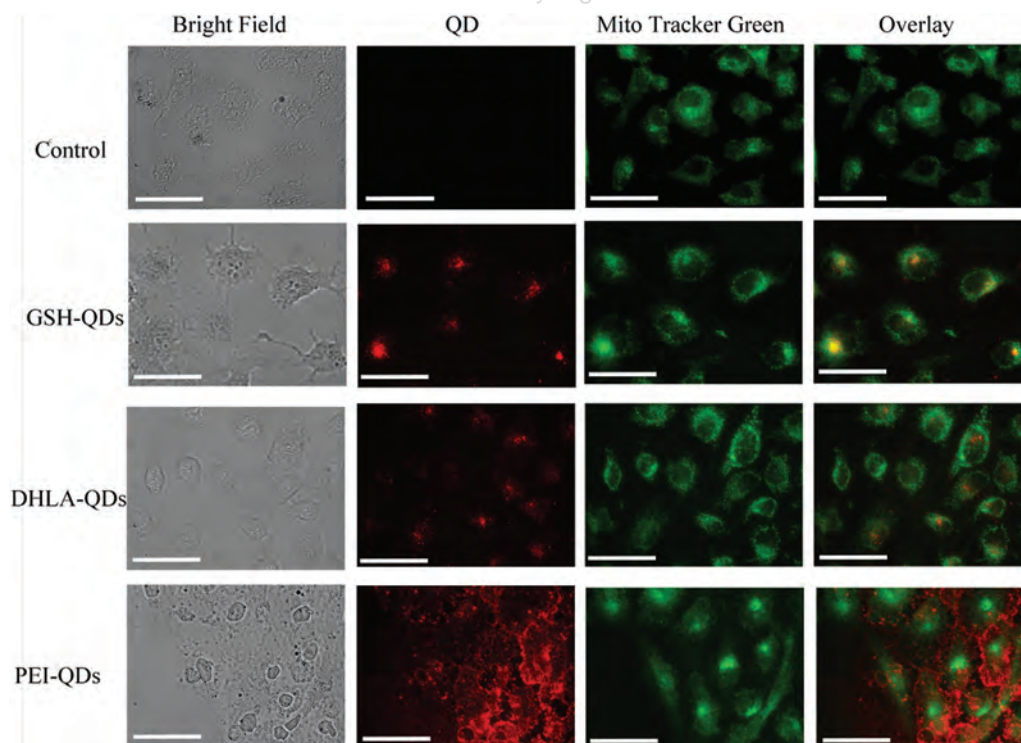

Figure 8. Subcellular localization of different ligands coated QDs with mitochondria in HaCaT cells after 24 h treatment (scale bars 25 μm).

this time if GSH-QDs enter the mitochondria via caveolae or by GSH specific transporters but the apparent localization of GSH-QD nanoparticles in mitochondria suggests a new strategy for targeting and releasing mitochondria-specific drugs/genes.[37]

Mitochondrial Targeting of GSH-QD in HaCaT Cells

Our present TEM findings suggest that GSH coating can mediate the cytosolic targeting of QDs to the mitochondria in HaCaT cells. To examine this further we conducted co-localization studies using a mitochondria specific marker (Mito Tracker green, Molecular Probes) that labels mitochondria green. Merged images of red QD fluorescence will appear yellow if the QDs are localized in the mitochondria. Results (Fig. 8) show clearly that only the GSH-QDs produce the co-localization signal. DHLA-QDs were dispersed between the mitochondria and there were no signal overlaps between the green and red, suggesting an absence of these nanoparticles within mitochondria. Similar results were obtained PEI-QDs, confirming the absence of co-localization between PEI-QDs and the mitochondrial marker.

CONCLUSIONS

In this study we investigated the effect of surface charge and coating chemistry of CdSe/ZnS core/shell QDs on the interaction of HaCaT keratinocytes in terms of ROS generation, cytotoxicity, cell uptake and subcellular localization. We prepared and characterized QDs modified by two positive ligands (CYS, PEI) and two negative ligands (GSH, DHLA). We observed significant differences in the extent and mode of QD uptake depending on the surface coatings. Positive charged QDs were taken up by a much greater extent than negative charged QDs. This is likely due to the electrostatic accumulation of positive QDs at the cell surface. Positive charged PEI-QD correspondingly induced higher cytotoxicity and ROS; however, the positive CYS-QDs cause considerably less ROS and less cytotoxicity which is likely due to the antioxidant characteristics of CYS. In addition, we investigated dependence of QD surface charge and coating composition on cell uptake and subcellular distribution. TEM studies showed evidence that all four types of QDs were endocytosed at the plasma membrane into vesicles but strong differences were observed post internalization. The preponderance of high positive CYS-QDs were observed as free aggregates in the cytosol whereas the positive PEI-QDs resided in fluid filled vesicles. The oxidative stress induced by the PEI-QDs was evident by the high presence of lipid droplets. Small clusters of negative charged DHLA-QDs were typically sequestered in cytosolic vesicles whereas we observed a targeting of negative charge GSH-QDs to mitochondria. This finding suggests the possibility that GSH coatings could be a general nanoparticle-based approach for

targeting and releasing mitochondria-specific drug/gene delivery.

REFERENCES

1. Y. P. Ho and K. W. Leong, Quantum dot-based theranostics. *Nanoscale* 2, 60 (**2009**).
2. W. C. Chan, D. J. Maxwell, X. Gao, R. E. Bailey, M. Han, and S. Nie, Luminescent quantum dots for multiplexed biological detection and imaging. *Curr. Opin. Biotechnol.* 13, 40 (**2002**).
3. X. Michalet, F. F. Pinaud, L. A. Bentolila, J. M. Tsay, S. Doose, J. J. Li, G. Sundaresan, A. M. Wu, S. S. Gambhir, and S. Weiss, Quantum dots for live cells, *in vivo* imaging, and diagnostics. *Science* 307, 538 (**2005**).
4. Y. Wang and L. Chen, Quantum dots, lighting up the research and development of nanomedicine. *Nanomedicine* 7, 385 (**2011**).
5. E. Hutter and D. Maysinger, Gold nanoparticles and quantum dots for bioimaging. *Microsc. Res. Tech.* 74, 592 (**2011**).
6. R. G. Aswathy, Y. Yoshida, T. Maekawa, and D. S. Kumar, Near-infrared quantum dots for deep tissue imaging. *Anal. Bioanal. Chem.* 397, 1417 (**2010**).
7. C. Wang, X. Gao, and X. Su, *In vitro* and *in vivo* imaging with quantum dots. *Anal. Bioanal. Chem.* 397, 1397 (**2010**).
8. R. Hardman, A toxicologic review of quantum dots: Toxicity depends on physicochemical and environmental factors. *Environ. Health Perspect.* 114, 165 (**2006**).
9. V. Mailander and K. Landfester, Interaction of nanoparticles with cells. *Biomacromolecules* 10, 2379 (**2009**).
10. A. Verma and F. Stellacci, Effect of surface properties on nanoparticle-cell interactions. *Small* 6, 12 (**2010**).
11. W. Jiang, B. Y. Kim, J. T. Rutka, and W. C. Chan, Nanoparticle-mediated cellular response is size-dependent. *Nat. Nanotechnol.* 3, 145 (**2008**).
12. S. E. Gratton, P. A. Ropp, P. D. Pohlhaus, J. C. Luft, V. J. Madden, M. E. Napier, and J. M. Desimone, The effect of particle design on cellular internalization pathways. *Proc. Natl. Acad. Sci. USA* 105, 11613 (**2008**).
13. D. Hühn, K. Kantner, C. Geidel, S. Brandholt, I. De Cock, S. J. H. Soenen, P. Rivera_Gil, J. M. Montenegro, K. Braeckmans, K. Müllen, G. U. Nienhaus, M. Klapper, and W. J. Parak, Polymer-coated nanoparticles interacting with proteins and cells: Focusing on the sign of the net charge. *ACS Nano* 7, 3253 (**2013**).
14. A. Asati, S. Santra, C. Kaittanis, and J. M. Perez, Surface-charge-dependent cell localization and cytotoxicity of cerium oxide nanoparticles. *ACS Nano* 4, 5321 (**2010**).
15. F. Variola, J. B. Brunski, G. Orsini, P. T. De Oliveira, R. Wazen, and A. Nanci, Nanoscale surface modifications of medically relevant metals: State-of-the art and perspectives. *Nanoscale* 3, 335 (**2011**).
16. F. Zhao, Y. Zhao, Y. Liu, X. Chang, and C. Chen, Cellular uptake, intracellular trafficking, and cytotoxicity of nanomaterials. *Small* 7, 1322 (**2011**).
17. X. Jiang, C. Rocker, M. Hafner, S. Brandholt, R. M. Dorlich, and G. U. Nienhaus, Endo- and exocytosis of zwitterionic quantum dot nanoparticles by live hela cells. *ACS Nano* 4, 6787 (**2010**).
18. A. E. Nel, L. Madler, D. Velegol, T. Xia, E. M. Hoek, P. Somasundaran, F. Klaessig, V. Castranova, and M. Thompson, Understanding biophysicochemical interactions at the nano-bio interface. *Nat. Mater.* 8, 543 (**2009**).

19. Y. Xiao, S. P. Forry, X. Gao, R. D. Holbrook, W. G. Telford, and A. Tona, Dynamics and mechanisms of quantum dot nanoparticle cellular uptake. *Journal of Nanobiotechnology* 8, 13 (**2010**).

20. L. W. Zhang and N. A. Monteiro-Riviere, Mechanisms of quantum dot nanoparticle cellular uptake. *Toxicol. Sci.* 110, 138 (**2009**).

21. M. J. Clift, B. Rothen-Rutishauser, D. M. Brown, R. Duffin, K. Donaldson, L. Proudfoot, K. Guy, and V. Stone, The impact of different nanoparticle surface chemistry and size on uptake and toxicity in a murine macrophage cell line. *Toxicol. Appl. Pharmacol.* 232, 418 (**2008**).

22. J. K. Jaiswal, H. Mattoussi, J. M. Mauro, and S. M. Simon, Long-term multiple color imaging of live cells using quantum dot bioconjugates. *Nat. Biotechnol.* 21, 47 (**2003**).

23. R. D. Holbrook, K. E. Murphy, J. B. Morrow, and K. D. Cole, Trophic transfer of nanoparticles in a simplified invertebrate food web. *Nat. Nanotechnol.* 3, 352 (**2008**).

24. H. Duan and S. Nie, Cell-penetrating quantum dots based on multivalent and endosome-disrupting surface coatings. *J. Am. Chem. Soc.* 129, 3333 (**2007**).

25. J. P. Ryman-Rasmussen, J. E. Riviere, and N. A. Monteiro-Riviere, Surface coatings determine cytotoxicity and irritation potential of quantum dot nanoparticles in epidermal keratinocytes. *J. Invest. Dermatol.* 127, 143 (**2007**).

26. W. W. Yu, L. Qu, W. Guo, and X. Peng, Experimental determination of the extinction coefficient of CdTe, CdSe, and CdS nanocrystals. *Chem. Mater.* 15, 2854 (**2003**).

27. D. Fischer, Y. Li, B. Ahlemeyer, J. Krieglstein, and T. Kissel, *In vitro* cytotoxicity testing of polycations: Influence of polymer structure on cell viability and hemolysis. *Biomaterials* 2, 1121 (**2003**).

28. R. K. Singhal, M. E. Anderson, and A. Meister, Glutathione, a first line of defense against cadmium toxicity. *FASEB J.* 1, 220 (**1987**).

29. M. Neu, D. Fischer, and T. Kissel, Recent advances in rational gene transfer vector design based on poly(ethylene imine) and its derivatives. *J. Gene. Med.* 7, 992 (**2005**).

30. P. Midoux, C. Pichon, J. J. Yaouanc, and P. A. Jaffrès, Chemical vectors for gene delivery: A current review on polymers, peptides and lipids containing histidine or imidazole as nucleic acids carriers. *British Journal of Pharmacology* 157, 166 (**2009**).

31. J. Boren and K. M. Brindle, Apoptosis-induced mitochondrial dysfunction causes cytoplasmic lipid droplet formation. *Cell Death and Differentiation* 19, 1561 (**2012**).

32. V. Ribas, C. García-Ruiz, and J. C. Fernández-Checa, Glutathione and mitochondria. *Frontiers in Pharmacology* 5, 151 (**2014**).

33. L. H. Lash, Mitochondrial glutathione transport: Physiological, pathological and toxicological implications. *Chemico-Biological Interactions* 163, 54 (**2006**).

34. P. V. AshaRani, G. Low Kah Mun, M. P. Hande, and S. Valiyaveettil, Cytotoxicity and genotoxicity of silver nanoparticles in human cells. *ACS Nano* 3, 279 (**2009**).

35. V. Soubannier, G. L. McLelland, R. Zunino, E. Braschi, P. Rippstein, E. A. Fon, and H. M. McBride, A vesicular transport pathway shuttles cargo from mitochondria to lysosomes. *Curr. Biol.* 22, 135 (**2012**).

36. H. N. Fridolfsson, D. M. Roth, P. A. Insel, and H. H. Patel, Regulation of intracellular signaling and function by caveolin. *FASEB J.* 28, 3823 (**2014**).

37. V. Weissig, Mitochondrial-targeted drug and DNA delivery. *Crit. Rev. Ther. Drug Carrier Syst.* 20, 1 (**2003**).